Jihun Han[1]
Energy Systems Division,
Argonne National Laboratory,
Lemont, IL 60439
e-mail: jihun.han@anl.gov

Dominik Karbowski
Energy Systems Division,
Argonne National Laboratory,
Lemont, IL 60439
e-mail: dkarbowski@anl.gov

Namdoo Kim
Energy Systems Division,
Argonne National Laboratory,
Lemont, IL 60439
e-mail: nkim@anl.gov

Aymeric Rousseau
Energy Systems Division,
Argonne National Laboratory,
Lemont, IL 60439
e-mail: arousseau@anl.gov

Human Driver Modeling Based on Analytical Optimal Solutions: Stopping Behaviors at the Intersections

Safe and energy-efficient driving of connected and automated vehicles (CAVs) must be influenced by human-driven vehicles. Thus, to properly evaluate the energy impacts of CAVs in a simulation framework, a human driver model must capture a wide range of real-world driving behaviors corresponding to the surrounding environment. This paper formulates longitudinal human driving as an optimal control problem with a state constraint imposed by the vehicle in front. Deriving analytically optimal solutions by employing optimal control theory can capture longitudinal human driving behaviors with low computational burden, and adding the state constraint can assist with describing car-following features while anticipating behaviors of the vehicle in front. We also use on-road testing data collected by an instrumented vehicle to validate the proposed human driver model for stop scenarios at intersections. Results show that vehicle stopping trajectories of the proposed model are well matched with those of experimental data. [DOI: 10.1115/1.4046575]

Keywords: automotive systems, dynamics and control, human dynamics, intelligent transportation systems, model validation, optimal controls

Introduction

Thanks to advanced vehicle technologies, vehicles can be connected with other vehicles and roadside infrastructure through communication, moreover they can be equipped with different levels of automation (e.g., levels 1–5). These connected and automated vehicles (CAVs) can be aware of the surrounding environment continuously and predict future situations accurately; thus, they can reduce collisions due to human errors through anticipative and cooperative car-following and save energy further through energy-efficient driving and powertrain operation. In recent years, this topic is rapidly growing, and many researchers have presented energy-efficient driving solutions for CAVs [1]. To evaluate the energy impacts of CAVs systematically, we have developed a new multi-vehicle tool, RoadRunner [2], which allows CAVs to interact with surrounding vehicles and infrastructure on real-world routes in a closed-loop fashion. Moreover, RoadRunner is based on AUTONOMIE [3], which is an established tool for examining vehicle energy consumption and performance, where powertrain models have been validated over 10 years using chassis dynamometer test data [4]. RoadRunner development is more timely now as it allows researchers to perform a large-scale analysis of the energy impacts of CAVs with high accuracy.

As a part of RoadRunner, human driver model development and validation are critical because simplified models may not capture detailed real-world vehicle state trajectories, moreover their unrealistic behaviors may exaggerate the energy-saving potential of CAVs. In the traffic flow research area, efforts have been devoted to developing microscopic and macroscopic traffic models that result from human driving behaviors since the 1950s. Generally, the microscopic models describe traffic flow from the point of individual drivers and vehicles, whereas macroscopic models describe the collective state in terms of spatiotemporal fields of the local density, speed, and flow [5]. A car-following component is a fundamental part of microscopic models, and this feature must be simple enough to compute quickly, while describing individual driving behaviors. Several papers provide a comprehensive and excellent survey on the car-following models [6–8]. According to these papers, the car-following models are divided into several types: stimulus-response models, desired measures models, safety-distance models, optimal velocity models, fuzzy logic models, and psycho-physical models, among others. Most of the models adjusting speed and/or distance to the vehicle in front work so well that they capture macroscopic aspects of traffic dynamics for a certain condition by aggregating individual trajectories. Furthermore, consideration of human factors resulting from imperfect control has led developers to improve their own models and present other types of car-following models [9,10].

In microscopic traffic simulation, there is no need to capture a wide range of individual trajectories if the macroscopic aspects are well captured within an acceptable level of accuracy. However, several papers pointed out that car-following models are not matched with experimental data even though they are calibrated [11,12]. The RoadRunner requires a simple but high-fidelity dynamic human driver model that can capture a wide range of different driving behaviors corresponding to individual driving style as well as the surrounding environment (e.g., traffic signal phase and timing), not limited to car-following behaviors. To this end, we assumed longitudinal human driving, and this assumption leads to the formulation of an optimal control problem minimizing jerk (the derivative of acceleration) energy. We derived analytical state-constrained optimal solutions as a function of driving-related parameters through Pontryagin's minimum principle (PMP) [13], thereby satisfying the simplicity to be computationally efficient, while replicating real-world human-driven vehicles including car-following features if necessary. Unlike existing car-following models that update acceleration by using the relative distance and speed, the proposed model based on the optimal solutions updates jerk by using more driving-related parameters, which diversifies driving behaviors and guarantees the continuity in acceleration trajectory when road events occur.

The paper is organized as follows: the section on the human driving problem introduces assumptions and formulates human driving as an optimal control problem. In the section on analytical

[1]Corresponding author.

Manuscript received October 23, 2019; final manuscript received February 12, 2020; published online March 4, 2020. Assoc. Editor: Kam K. Leang.

solutions, we address derivations of analytical optimal solutions and show several case studies. In the section on validation, the proposed model is validated through experimental data. Finally, in the last section, the conclusions and future work resulting from this paper are discussed.

Longitudinal Human Driving Problem

Assumptions. We assume that drivers basically prioritize driving comfort, while avoiding any collisions with the vehicle in front and obeying traffic rules; maximizing driving comfort is considered as minimizing total jerk energy. As human drivers are able to anticipate behaviors of the vehicle in front of them, they plan and apply the control decision, such an anticipation is based on the assumption that the vehicle in front travels at the constant acceleration in a predictive time interval. Furthermore, vehicle longitudinal dynamics is simplified to the triple-integrator model by neglecting aerodynamic drag, road grade, etc. These assumptions facilitate derivation of analytical optimal solutions, which can be computed quickly. Anticipation, planning, and control decision are made at every time instant until arriving at the destination.

Optimal Control Problem Formulation. Let us define a control variable u as jerk j. A cost function to minimize total jerk energy over the predictive time interval T is

$$J = \min_{u} \int_{t_k}^{t_k+T} \left(l = \frac{1}{2}u^2 \right) dt \tag{1}$$

where t_k is a current time. Furthermore, we consider a vehicle longitudinal dynamics model as the triple-integrator model

$$\dot{s} = v, \quad \dot{v} = a, \quad \dot{a} = j = u \tag{2}$$

where a system dynamics $f = [v, a, u]^\top$, and a state vector $x = [s, v, a]^\top$.

To avoid collisions with the vehicle in front, the position of the driver's vehicle with a desired distance gap s_d must be smaller than the position of the vehicle in front s_p. Thus, a state variable inequality constraint (SVIC) h is defined as

$$h(t) = s + s_d - s_p = s + (v\tau + s_s) - s_p \leq 0 \tag{3}$$

where $s_d = s_s + v\tau$, τ is a desired time headway, which is the arriving time difference at the same point between successive vehicles, and s_s is the minimum safety distance gap at standstill conditions. Note that desired speed gap and acceleration gap are $v_d = s_s + a\tau$ and $a_d = u\tau$, respectively. Using assumptions made in the previous section, s_p can be expressed as $s_p = s_{p.k} + v_{p.k}t + \frac{1}{2}a_{p.k}t^2$, where $s_{p.k} = s_p(t_k)$, $v_{p.k} = v_p(t_k)$, and $a_{p.k} = a_p(t_k)$.

Boundary conditions are

$$\begin{aligned} &s(t_k) = s_k, \quad v(t_k) = v_k, \quad a(t_k) = a_k, \\ &s(t_k + T) = s_f, \quad v(t_k + T) = v_f, \quad a(t_k + T) = a_f \end{aligned} \tag{4}$$

where T is fixed. For simplicity, without loss of generality, $t_k = 0$ and $k = 0$ in the remainder of the paper.

Pontryagin's Minimum Principle With SVIC. To handle SVIC, we use a direct adjoining method [14] as it directly adjoins the SVIC in the Hamiltonian and provides the optimality conditions for the optimal solution through PMP; its optimality conditions are independent of the order of a pure SVIC form $h(x, t) \leq 0$ in which u does not explicitly appear, where the order p is defined by $h_u^{(p)} = \partial / \partial u \left(d^p / dt^p h \right) \neq 0$, $h_u^{(i)} = 0$ for $i = 1, \ldots, p-1$. When the SVIC is active, there may exist a sub-interval satisfying $h(x, t) = 0$ for $t \in [t_1, t_2]$ with $t_1 < t_2$, called a boundary interval (t_1 and t_2 are entry time and exit time, respectively) or a point satisfying $h(x, t_1) = 0$, called a contact point (t_1 is contact time). Note that the entry, exit, and contact times are called junction times.

Hamiltonian H is defined first, and then a Lagrangian multiplier η is used to directly adjoin the SVIC to H in order to form Lagrangian L

$$H = l + \lambda^\top f, \quad L = H + \eta h \tag{5}$$

where λ are co-state variables and l has the same definition as in Eq. (1). The optimality condition is

$$L_u = 0, \quad \dot{\lambda} = -L_x \tag{6}$$

where $\eta \geq 0, \eta h = 0$. Jump conditions at junction times t_j with a jump parameter π are

$$\lambda(t_j^-) = \lambda(t_j^+) + \pi h_x(x, t_j), \quad H(t_j^-) = H(t_j^+) - \pi h_t(x, t_j) \tag{7}$$

where $\pi \geq 0, \pi h = 0$, and t_j^- and t_j^+ indicate the left-hand side and the right-hand side of t_j, respectively.

Analytical Solutions

From the optimal control problem formulated by Eqs. (1), (2), (3), and (4), we define H and L as

$$\begin{aligned} H &= \frac{1}{2}u^2 + \lambda_s v + \lambda_v a + \lambda_a u \\ L &= H + \eta \left(s + v\tau + s_s - s_{p.0} - v_{p.0}t - \frac{1}{2}a_{p.0}t^2 \right) \end{aligned} \tag{8}$$

Then, an optimal control policy is derived by the optimality condition as follows: $u^*(t) = -\lambda_a$. Co-state dynamics with jump conditions are derived as

$$\begin{aligned} &\dot{\lambda}_s = -\eta && \text{with } \lambda_s(t_j^-) = \lambda_s(t_j^+) + \pi \\ &\dot{\lambda}_v = -\lambda_s - \eta\tau && \text{with } \lambda_v(t_j^-) = \lambda_v(t_j^+) + \pi\tau \\ &\dot{\lambda}_a = -\lambda_v && \text{with } \lambda_a(t_j^-) = \lambda_a(t_j^+) \end{aligned} \tag{9}$$

where $h = 0$ and $\pi \neq 0$ if the SVIC is active, that is position and speed co-states must have a discontinuity at junction times, whereas the acceleration co-state is always continuous; otherwise, $\eta = 0$ and $\pi = 0$.

From $h = 0$ and the last condition in Eq. (7), we add the constraints

$$\begin{aligned} &s(t_j) + (s_s + v(t_j)\tau) - s_{p.0} - v_{p.0}t_j - \frac{1}{2}a_{p.0}t_j^2 = 0 \\ &v(t_j) + a(t_j)\tau - v_{p.0} - a_{p.0}t_j = 0 \end{aligned} \tag{10}$$

The SVIC here is of the second order; thus, when the SVIC becomes tighter, a contact point occurs first and then a boundary interval occurs (e.g., a decrease in $s_{p.0}$ gives the same conditions), which is theoretically proven in Ref. [15]. Therefore, to retain states on the boundary interval, the following constraint is also satisfied:

$$a(t_j) + u(t_j)\tau - a_{p.0} = 0 \tag{11}$$

Lastly, terminal state equality constraints (TSECs) from Eq. (4) are

$$s(T) - s_f = 0, \quad v(T) - v_f = 0, \quad a(T) - a_f = 0 \tag{12}$$

where $v_f = a_f = 0$ for stop scenarios.

In summary, boundary conditions determine whether and how SVIC is active, thus analytical solutions consist of three types: type 1 (inactive SVIC), type 2 (active SVIC at contact point), and type 3 (active SVIC on boundary interval). We heuristically determine an appropriate solution type. If type 1 does not violate the SVIC, then it is applied; otherwise, we check if there exists one feasible contact point for type 2. After this identification, if type 2 is

feasible then it is applied; otherwise, type 3 is applied. The detailed description for all types of solutions is written as follows:

Type 1: Inactive SVIC. When the SVIC is inactive, $\eta = 0$. Thus, the optimal co-states are derived using Eq. (9)

$$\begin{aligned}\lambda_s^*(t) &= \lambda_{s.0}\\ \lambda_v^*(t) &= -\lambda_{s.0}t + \lambda_{v.0}\\ \lambda_a^*(t) &= \frac{1}{2}\lambda_{s.0}t^2 - \lambda_{v.0}t + \lambda_{a.0}\end{aligned} \tag{13}$$

where $\lambda_{s.0} = \lambda_s^*(0)$, $\lambda_{v.0} = \lambda_v^*(0)$, and $\lambda_{a.0} = \lambda_a^*(0)$, while superscript * indicates optimal. Using the optimal control policy, it is possible to integrate the state dynamics in Eq. (2). Then, we obtain a system of three linear equations with three unknown variables ($\lambda_{s.0}$, $\lambda_{v.0}$, and $\lambda_{a.0}$). By enforcing the TSECs in Eq. (12), a solution to this system is

$$\begin{aligned}\lambda_{s.0} &= \frac{720(s_0 - s_f)}{T^5} + \frac{360(v_0 + v_f)}{T^4} + \frac{60(a_0 - a_f)}{T^3}\\ \lambda_{v.0} &= \frac{360(s_0 - s_f)}{T^4} + \frac{192v_0 + 168v_f}{T^3} + \frac{36a_0 - 24a_f}{T^2}\\ \lambda_{a.0} &= \frac{60(s_0 - s_f)}{T^3} + \frac{36v_0 + 24v_f}{T^2} + \frac{9a_0 - 3a_f}{T}\end{aligned} \tag{14}$$

Finally, we get $a^*(t) = -\int\lambda_a + a_0$, $v^*(t) = \int a^* + v_0$, and $s^*(t) = \int v^* + s_0$. Note that the above solution was also used in Ref. [16].

Type 2: Active SVIC at Contact Point. When the SVIC is active at a contact time t_1, position and speed co-states jump to different values; thus, the resulting co-state trajectories with $\eta = 0$ consist of two intervals as follows:

$$\begin{aligned}\lambda_s^*(t) &= \begin{Bmatrix}\lambda_{s.0} & t \in [0, t_1^-]\\ \lambda_{s.1}^+ & t \in [t_1^+, T]\end{Bmatrix}\\ \lambda_v^*(t) &= \begin{Bmatrix}-\lambda_{s.0}t + \lambda_{v.0} & t \in [0, t_1^-]\\ -\lambda_{s.1}^+(t - t_1) + \lambda_{v.1}^+ & t \in [t_1^+, T]\end{Bmatrix}\\ \lambda_a^*(t) &= \begin{Bmatrix}\frac{\lambda_{s.0}}{2}t^2 - \lambda_{v.0}t + \lambda_{a.0} & t \in [0, t_1^-]\\ \frac{\lambda_{s.1}^+}{2}(t - t_1)^2 - \lambda_{v.1}^+(t - t_1) + \lambda_{a.1}^+ & t \in [t_1^+, T]\end{Bmatrix}\end{aligned} \tag{15}$$

where $\lambda_{s.1}^+ = \lambda_s^*(t_1^+) = \lambda_s^*(t_1^-) - \pi$, $\lambda_{v.1}^+ = \lambda_v^*(t_1^+) = \lambda_v^*(t_1^-) - \pi\tau$, and $\lambda_{a.1}^+ = \lambda_a^*(t_1^+) = \lambda_a^*(t_1^-)$ from the jump conditions in Eq. (9). In the same way as in type 1, the state dynamics are integrated; but here, two interior-point constraints at t_1 from Eq. (10) must be additionally satisfied. For this reason, we obtain a system of five nonlinear equations with five unknown variables ($\lambda_{s.0}$, $\lambda_{v.0}$, $\lambda_{a.0}$, π, and t_1) as follows:

$$\begin{aligned}&s^*(t_1) + s_s + v^*(t_1)\tau - s_{p.0} - v_{p.0}t_1 - \frac{1}{2}a_{p.0}t_1^2 = 0\\ &v^*(t_1) + a^*(t_1)\tau - v_{p.0} - a_{p.0}t_1 = 0\\ &\text{TSECs in Eq. (12)}\end{aligned} \tag{16}$$

By solving the first four equations, we derive four variables ($\lambda_{s.0}$, $\lambda_{v.0}$, $\lambda_{a.0}$, π) as a function of t_1, and then substitute them into the last equation to obtain one-ninth order of polynomial with one variable of t_1. From such a polynomial, we can compute a feasible t_1 satisfying a condition of $0 \le t_1 \le T$.

Type 3: Active SVIC on Boundary Interval. When the SVIC is active on the boundary interval $[t_1, t_2]$, there are two jumps in position and speed co-states with jump parameters π_1 and π_2 at t_1 and t_2, respectively. The η is no longer zero and dominates co-state dynamics as the three constraints in Eqs. (10) and (11) must be held on $[t_1, t_2]$. After the third constraint is differentiated one time with respect to t, we substitute λ_a for u using the optimal control policy and obtain the following explicit solution:

$$\lambda_a^*(t) = \lambda_{a.1}^+ e^{-(t-t_1)/\tau} \tag{17}$$

where $\lambda_{a.1}^+ = \lambda_a^*(t_1^+) = \lambda_a^*(t_1^-)$. Using the above formula and the co-state dynamics in Eq. (9), we obtain the explicit solutions of other co-states as well:

$$\begin{aligned}\lambda_s^*(t) &= \lambda_{s.1}^+ e^{(t-t_1)/\tau} + c\lambda_{a.1}^+(e^{-(t-t_1)/\tau} - e^{(t-t_1)/\tau})\\ \lambda_v^*(t) &= \frac{1}{\tau}\lambda_{a.1}^+ e^{-(t-t_1)/\tau}\end{aligned} \tag{18}$$

with $\eta^*(t) = -(1/\tau)\lambda_s^*(t) + (1/\tau^3)\lambda_a^*(t)$, where $c = 1/2\tau^2$ and $\lambda_{s.1}^+ = \lambda_s^*(t_1^-) - \pi_1$. As $\lambda_v^*(t_1^+) = (1/\tau)\lambda_{a.1}^+$, the jump parameter π_1 from Eq. (9) is obtained as $\pi_1 = (1/\tau)\lambda_{v.1}^- - (1/\tau^2)\lambda_{a.1}^+$. Based on the above boundary interval control, we summarize

$$\begin{aligned}\lambda_s^*(t) &= \begin{Bmatrix}\lambda_{s.0} & t \in [0, t_1^-]\\ \text{1st Eq. (18)} & t \in [t_1^+, t_2^-]\\ \lambda_{s.2}^+ & t \in [t_2^+, T]\end{Bmatrix}\\ \lambda_v^*(t) &= \begin{Bmatrix}-\lambda_{s.0}t + \lambda_{v.0} & t \in [0, t_1^-]\\ \text{2nd Eq. (18)} & t \in [t_1^+, t_2^-]\\ -\lambda_{s.2}^+(t - t_2) + \lambda_{v.2}^+ & t \in [t_2^+, T]\end{Bmatrix}\\ \lambda_a^*(t) &= \begin{Bmatrix}\frac{1}{2}\lambda_{s.0}t^2 - \lambda_{v.0}t + \lambda_{a.0} & t \in [0, t_1^-]\\ \text{Eq. (17)} & t \in [t_1^+, t_2^-]\\ \frac{1}{2}\lambda_{s.2}^+(t - t_2)^2 - \lambda_{v.2}^+(t - t_2) + \lambda_{a.2}^+ & t \in [t_2^+, T]\end{Bmatrix}\end{aligned} \tag{19}$$

where $\lambda_{s.2}^+ = \lambda_s^*(t_2^-) - \pi_2$, $\lambda_{v.2}^+ = \lambda_v^*(t_2^-) - \pi_2\tau$, and $\lambda_{a.2}^+ = \lambda_a^*(t_2^-)$. Similarly, we obtain a system of six nonlinear equations with six unknown variables ($\lambda_{s.0}$, $\lambda_{v.0}$, $\lambda_{a.0}$, π_2, t_1, and t_2):

$$\begin{aligned}&s^*(t_1) + s_s + v^*(t_1)\tau - s_{p.0} - v_{p.0}t_1 - \frac{1}{2}a_{p.0}t_1^2 = 0\\ &v^*(t_1) + a^*(t_1)\tau - v_{p.0} - a_{p.0}t_1 = 0\\ &a^*(t_1) + u^*(t_1)\tau - a_{p.0} = 0\\ &\text{TSECs in Eq. (12)}\end{aligned} \tag{20}$$

After replacing four variables ($\lambda_{s.0}$, $\lambda_{v.0}$, $\lambda_{a.0}$, and π_2) in the last two equations, we can compute the remaining variables t_1 and t_2 satisfying a condition of $0 \le t_1 \le t_2 \le T$.

Simulation Studies. This section considers typical stop scenarios in the presence of the vehicle in front. We assume that the vehicle in front decelerates at the constant value and its initial setup is $a_{p.0} = -0.5$ m/s^2, $v_{p.0} = 10$ m/s, and $s_{p.0} = [60, 50, 40]^\top$ m. For host vehicle, its initial setup is $a_0 = -0.2$ m/s^2, $v_0 = 20$ m/s, $s_0 = 0$ m, $a_f = 0$ m/s^2, $v_f = 0$ m/s, $s_f = 100$ m, $T = 10$ s, $\tau = 1.2$ s, and $s_s = 2$ m.

In Fig. 1, the vehicle in front does not affect the driving behavior of the host vehicle. All co-state trajectories of type 1 are continuous, and the resulting optimal control policy enables the host vehicle to decelerate its speed for a stop in a way that minimizes total jerk energy. However, as initial distance gap decreases (i.e., $s_{p.0}$ decreases), the desired position trajectory ($s + s_d$) of the host vehicle starts surpassing the position trajectory of the vehicle in front (s_p) and then an actual rear-collision event occurs unless state-constrained solutions are used. As shown in Fig. 2, both position and speed co-states of type 2 are discontinuous at the contact time, which allows the desired position and speed of the host vehicle to match with the position and speed of the vehicle in front, respectively. On the other hand, the acceleration co-state is always continuous, which leads to a continuous optimal control policy. Lastly, in Fig. 3, type 3 builds up the boundary interval, jumps in the position,

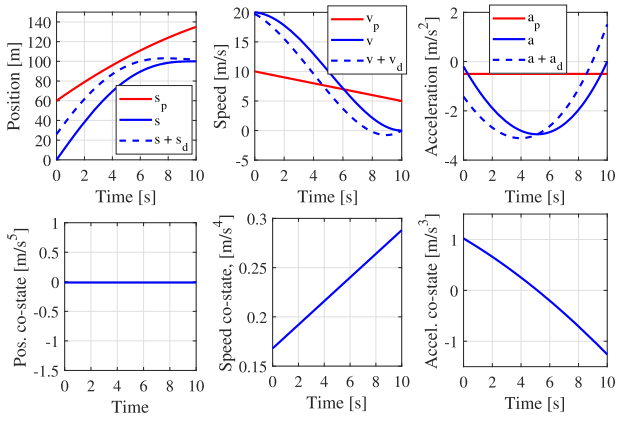

Fig. 1 State and co-state trajectories of type 1

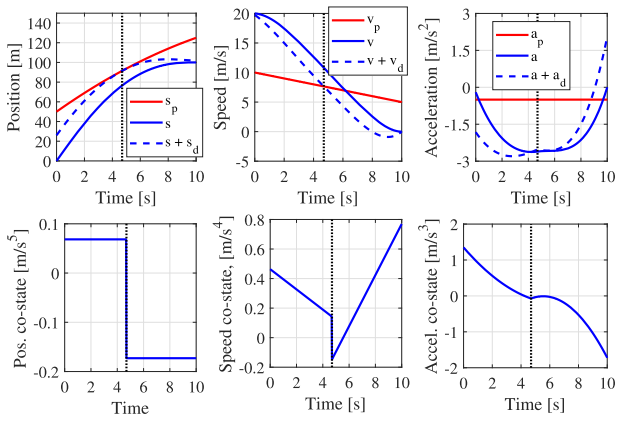

Fig. 2 State and co-state trajectories of type 2. Black dotted line represents the contact point.

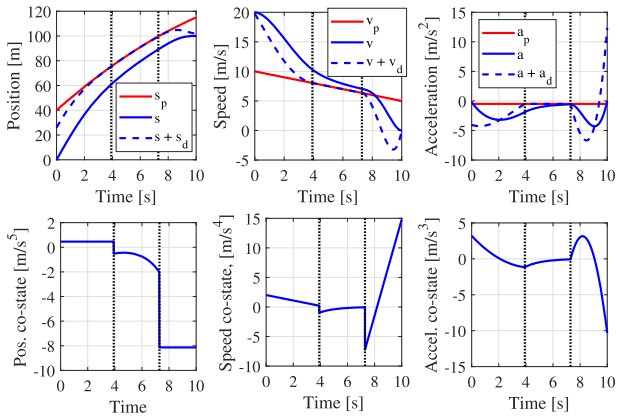

Fig. 3 State and co-state trajectories of type 3. Two black dotted lines represent entry and exit time, respectively.

and speed co-states occur at both entry and exit times, whereas the acceleration co-state is continuous. Notably, co-state dynamics on the boundary interval are influenced by η, which are different from that on other intervals, so that desired states of the host vehicle behave in exactly the same way as the vehicle in front.

Validation With Experimental Data

Experimental data were collected from an instrumented vehicle driven by a human driver and equipped with a dash video camera, global positioning system tracker, and a radar and then processed to make the data usable for validation. On-road testing was

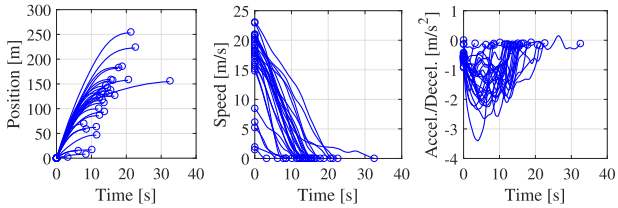

Fig. 4 Various trajectories of the braking regime from experimental dataset

performed on specific sub-urban route near Argonne, and the conditions at that time are light traffic, mostly sunny day, dry road condition, normal driving style, etc.

In this paper, we considered a braking regime only for stop scenarios near the intersections, including situations with and without the vehicle in front. From the experimental data, the parameters required by the human driver model (i.e., boundary conditions) were obtained: braking distance ($s_f - s_0$), braking time (T), and vehicle states at the timing to start braking (a_0 and v_0). As a result of how drivers respond to surrounding environment (e.g., traffic signal phase and timing), we could have various stopping trajectories as shown in Fig. 4. For car-following parameters, $s_s = 2$ m and $\tau = \min(1, s_{p.0} - s_s - s_0/v_0)$ s. Note that τ could be optimally researched in a way to minimize the error between the model and data.

To validate the model, we used two measures: (1) normalized cross correlation power (NCCP) [17] and (2) normalized root-mean-squared error (NRMSE) [11]. The NCCP and NRMSE are defined as

$$\text{NCCP} = \frac{\max\left[R_{xy}(\tau)\right]}{\max\left[R_{xx}(\tau), R_{yy}(\tau)\right]} \times 100$$
$$\text{NRMSE} = \frac{\sqrt{\sum_{i=0}^{T}(x_i - y_i)^2/T}}{(y_{\max} - y_{\min})} \times 100 \tag{21}$$

where $R_{xy}(\tau) = \lim_{T\to\infty}\int_0^T x(t) \circ y(t-\tau)dt$, and x and y represent speed signals of the model and data, respectively, while $y_{\max}$ and $y_{\min}$ are maximum and minimum values, respectively. Note that the NCCP value larger than 90% indicates that the two speed signals are highly correlated. Moreover, we also compared the proposed model with the intelligent driver model (IDM), well-known car-following model, with prescribed parameters, where the comfortable acceleration and deceleration are set to 1 and 1.5 m/s^2, the minimum spacing, the desired time headway, and desired speed are set to s_s, τ, and v_0, and the exponent is set to 4.

In Fig. 5, for the proposed model and IDM, all NCCP values are larger than 90% and all NRMSE values are less than 10% (except for IDM in the case number 28). The proposed model outperforms IDM as the average value of both measures is 98.6% versus 95.4% in NCCP, and 2.33% versus 5.39% in NRMSE. Figure 6 shows two specific cases including car-following situations to see how the host vehicle adjusts its driving behaviors, where values of a pair (NCCP, NRMSE) are (97.8%, 4.68%) versus (91.5%, 9.94%) for case number 18 (left) and (99.9%, 1.58%) versus (98.6%, 2.41%) for case number 22 (right). In case number 18, the surrounding vehicle changes its lane at about 10 s and drives in front of the equipped vehicle, which causes a discontinuity in trajectories (red line). Note that the relative position is set to 250 m and relative speed is set to zero if the radar sensor detects nothing in the same lane. If there are no vehicles in front, IDM maintains constant speed from 0 s to 3 s, but it starts braking, which jumps the negative value from zero acceleration, because of considering a red traffic light as a standing object. At about 10 s, IDM is too close to the cut-in vehicle, thus it must have the maximum braking rate,

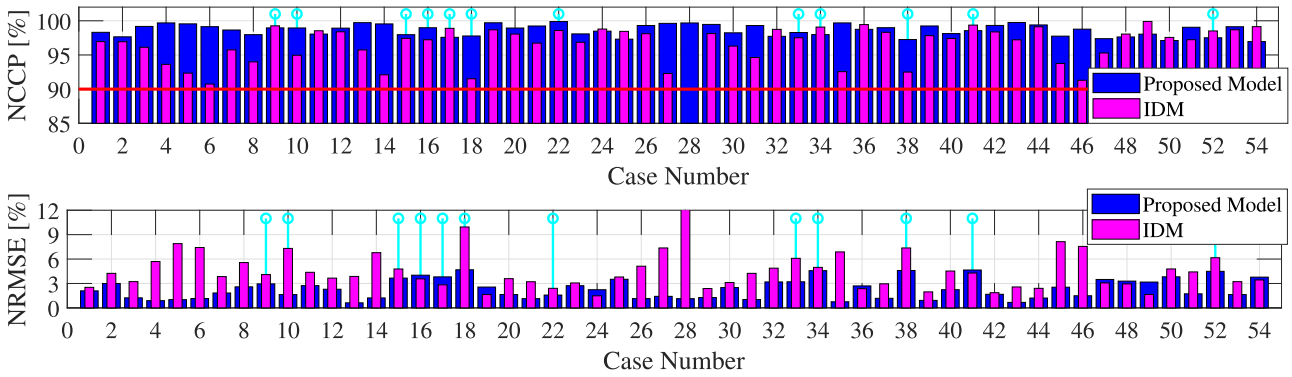

Fig. 5 NCCP and NRMSE of the proposed model (blue bar) and IDM (magenta bar) for 54 braking-to-stop cases. Vertical cyan lines represent for car-following situations.

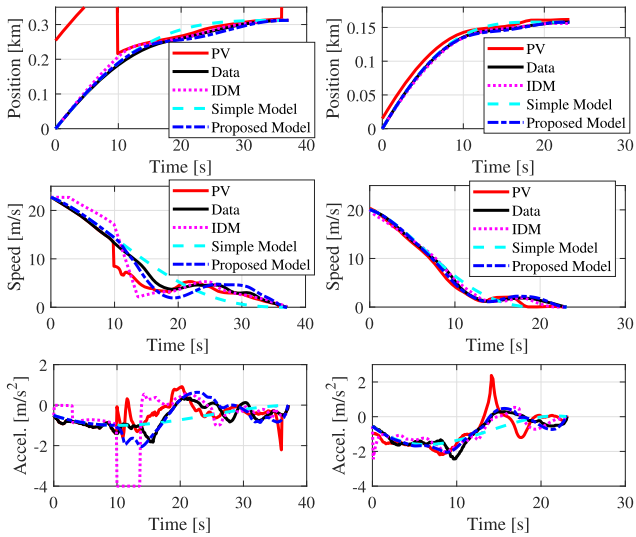

Fig. 6 Comparison of state trajectories between models and data in case numbers 18 (left) and 22 (right). PV is the preceding vehicle, and the simple model is the model using only type 1 solution that cannot describe the car-following feature.

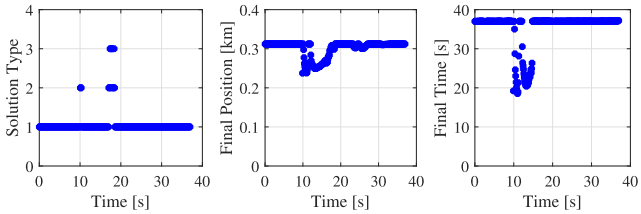

Fig. 7 Solution type, final position, and final time trajectories in case number 18

which is set by 4 m/s^2, leading to the large discrepancy in trajectories compared to the testing data.

However, the proposed model can set different braking times (e.g., 37 s and 23 s in case numbers 18 and 22, respectively) and its trajectory is quite close to that of the experimental data, while describing the car-following feature without a discontinuity in acceleration trajectory when road event occurs (e.g., traffic signal state switches to red, the vehicle in front appears), as shown in Fig. 6. Note that the simple model uses only type 1 solution, thereby unrealistically overtaking the vehicle in front in the same lane. As shown in Fig. 7, the boundary conditions must be adjusted to ensure that they are feasible to compute analytical optimal solutions depending on driving behavior of the vehicle in front (e.g., a final position with the desired distance gap cannot be larger than the anticipated final position of the vehicle in front if there is no lane-change) [18]. Both cases adjust boundary conditions; however, case number 18 must use the state-constrained solutions, whereas case number 22 does not.

Conclusions and Future Work

In this paper, we present a new approach for human driver modeling using an optimal control theory. The human driver is modeled based on analytical optimal solutions that maximize driving comfort for given boundary conditions, while considering the state constraint imposed by the vehicle in front. The proposed model is not only computationally efficient but also captures various stopping trajectories including car-following to keep the desired distance gap because its inputs (boundary conditions) directly represent one aspect of the driving behavior (e.g., braking time indicates braking level), respectively. Using experimental data, the proposed model is validated and also compared with IDM. Results show that the average values of NCCP and NRMSE for 54 braking-to-stop cases are about 98.6% and 2.33%, respectively, which indicates that the stopping behavior of the proposed model is highly correlated with that of the experimental data. The proposed model improves accuracy over IDM without a discontinuity which is seen in IDM when the road event occurs.

In future work, we would like to expand driving regimes (e.g., accelerating and cruising), rather than only focusing on braking, and we also consider road characteristics (such as curvature) to capture the speed reduction. We also would like to investigate if the proposed model can capture macroscopic aspects under high traffic conditions. Furthermore, another future research direction is to develop a model of perception and decision that can provide the timing and duration of each driving regime.

Acknowledgment

This report and the work described were sponsored by the U.S. Department of Energy (DOE) Vehicle Technologies Office (VTO) under the Systems and Modeling for Accelerated Research in Transportation (SMART) Mobility Laboratory Consortium, an initiative of the Energy Efficient Mobility Systems (EEMS) Program. DOE Office of Energy Efficiency and Renewable Energy (EERE) manager David Anderson played an important role in establishing the project concept, advancing implementation, and providing ongoing guidance.

Conflict of Interest

The submitted article has been created by UChicago Argonne, LLC, Operator of Argonne National Laboratory ("Argonne").

Argonne, a U.S. Department of Energy Office of Science laboratory, is operated under Contract No. DEAC02-06CH11357. The U.S. Government retains for itself, and others acting on its behalf, a paid-up nonexclusive, irrevocable worldwide license in said article to reproduce, prepare derivative works, distribute copies to the public, and perform publicly, and display publicly, by or on behalf of the Government.

Nomenclature

T = predictive time interval
s_s = minimum safety distance gap at standstill conditions
t_i = contact time if $i = 1$ or entry and exit times if $i = 1, 2$
s, v, a, j = position, speed, acceleration, and jerk
s_p, v_p, a_p = position, speed, and acceleration of the vehicle in front
s_d, v_d, a_d = desired distance, speed, and acceleration gaps
s_f, v_f, a_f = final position, final speed, and final acceleration
$u\ (:= j)$ = control input variable (:= jerk)
H, L = Hamiltonian and Lagrangian
η = Lagrange multiplier to directly adjoin the state constraint
$\lambda_s, \lambda_v, \lambda_s$ = position, speed, and acceleration co-state variables
π = jump parameter in co-state variables
τ = desired time headway

References

[1] Vahidi, A., and Sciarretta, A., 2018, "Energy Saving Potentials of Connected and Automated Vehicles," Transp. Res. Part C: Emerg. Technol., **95**, pp. 822–843.
[2] Kim, N., Karbowski, D., and Rousseau, A., 2018, "A Modeling Framework for Connectivity and Automation Co-Simulation," SAE Technical Paper 2018-01-0607.
[3] Argonne National Laboratory, 2017, AUTONOMIE (computer software).
[4] Kim, N., Duoba, M., Kim, N., and Rousseau, A., 2013, "Validating Volt PHEV Model With Dynamometer Test Data Using Autonomie," SAE Int. J. Passenger Cars Mech. Syst., **6**(2), pp. 985–992.
[5] Treiber, M., and Kesting, A., 2013, *Traffic Flow Dynamics*, Springer, Berlin.
[6] Brackstone, M., and McDonald, M., 1999, "Car-Following: A Historical Review," Transp. Res. Part F: Traffic Psychol. Behav., **2**(4), pp. 181–196.
[7] Toledo, T., 2007, "Driving Behaviour: Models and Challenges," Transp. Rev., **27**(1), pp. 65–84.
[8] Saifuzzaman, M., and Zheng, Z., 2014, "Incorporating Human-Factors in Car-Following Models: A Review of Recent Developments and Research Needs," Transp. Res. Part C: Emerg. Technol., **48**, pp. 379–403.
[9] Ro, J. W., Roop, P. S., Malik, A., and Ranjitkar, P., 2018, "A Formal Approach for Modeling and Simulation of Human Car-Following Behavior," IEEE Trans. Intell. Transp. Syst., **19**(2), pp. 639–648.
[10] Lindorfer, M., Mecklenbrauker, C. F., and Ostermayer, G., 2018, "Modeling the Imperfect Driver: Incorporating Human Factors in a Microscopic Traffic Model," IEEE Trans. Intell. Transp. Syst., **19**(9), pp. 2856–2870.
[11] Wagner, P., 2005, "Empirical Description of Car-Following," *Traffic and Granular Flow '03*, Hoogendoorn, S. P., Luding, S., Bovy, P. H. L., Schreckenberg, M., and Wolf, D. E., eds., Springer, Berlin, pp. 15–27.
[12] Sangster, J., Rakha, H., and Du, J., 2013, "Application of Naturalistic Driving Data to Modeling of Driver Car-Following Behavior," Transp. Res. Record: J. Transp. Res. Board, **2390**(1), pp. 20–33.
[13] Pontryagin, L., 1987, *Mathematical Theory of Optimal Processes*, 1st ed., Routledge, London.
[14] Hartl, R. F., Sethi, S. P., and Vickson, R. G., 1995, "A Survey of the Maximum Principles for Optimal Control Problems With State Constraints," SIAM Rev., **37**(2), pp. 181–218.
[15] Hamilton, W., 1972, "On Nonexistence of Boundary Arcs in Control Problems With Bounded State Variables," IEEE Trans. Automat. Control, **17**(3), pp. 338–343.
[16] Da Lio, M., Mazzalai, A., Gurney, K., and Saroldi, A., 2018, "Biologically Guided Driver Modeling: The Stop Behavior of Human Car Drivers," IEEE Trans. Intell. Transp. Syst., **19**(8), pp. 2454–2469.
[17] Meng, Y., Jennings, M., Tsou, P., Brigham, D., Bell, D., and Soto, C., 2011, "Test Correlation Framework for Hybrid Electric Vehicle System Model," SAE Int. J. Eng., **4**(1), pp. 1046–1057.
[18] Han, J., Sciarretta, A., Ojeda, L. L., De Nunzio, G., and Thibault, L., 2018, "Safe- and Eco-Driving Control for Connected and Automated Electric Vehicles Using Analytical State-Constrained Optimal Solution," IEEE Trans. Intell. Veh., **3**(2), pp. 163–172.